Analysis and Design of an LCL-T Resonant Converter as a Constant-Current Power Supply

Mangesh Borage, Sunil Tiwari, and Swarna Kotaiah

***Abstract*—An LCL-T resonant converter (LCL-T RC) is shown to behave as a current source when operated at resonant frequency. A detailed analysis of the LCL-T RC for this property is presented. Closed-form expressions for converter gain, component stresses, and the condition for converter design optimized for minimum size of resonant network is derived. A design procedure is illustrated with a prototype 200-W 20-A current-source power supply and experimental results are presented. The LCL-T RC as a current source offers many advantages such as easy parallel operation and low circulating currents at light load. Additionally, with appropriate phase shift in paralleled modules, the peak–peak ripple in output current is reduced and the ripple frequency is increased, reducing filtering requirements. The leakage inductance of a transformer can be advantageously integrated into the resonant network. These merits make the topology applicable in various applications such as magnet power supply, capacitor charging power supply, laser diode drivers, etc.**

***Index Terms*—Current supplies, dc–dc power conversion, resonant power conversion, soft switching.**

NOMENCLATURE

A	A term defined by (13).
C	Capacitance value of resonant capacitor, C.
$E_{\rm n}$	Normalized total inductor energy.
f	Switching frequency.
$f_{\rm o}$	Resonant frequency.
H	Current gain.
$I_{\rm B}$	Base current.
$I_{C,\rm rms}$	RMS value of current in capacitor C.
$I_{C\rm N}$	Normalized rms current in capacitor C.
$I_{L,\rm rms}$	RMS value of current in inductor L.
$I_{L\rm N}$	Normalized rms current in inductor L.
$I_{L_a,\rm rms}$	RMS value of current in inductor L_a.
$I_{L_a\rm N}$	Normalized rms current in inductor L_a.
$I_{\rm o}$	Output dc current.
L	Inductance value of resonant inductor L.
L_a	Inductance value of resonant inductor L_a.
M	Voltage gain.
N_1	Number of primary turns in transformer.
N_2	Number of secondary turns in transformer.
p	Number of parallel-connected converters.
Q	The Q-value of the resonant circuit.
$Q_{\rm opt}$	Optimum value of Q.
$R_{\rm ac}$	Equivalent ac resistance.
$R_{\rm L}$	Load resistance.
$V_{\rm B}$	Base voltage.
$V_{C,\rm rms}$	RMS value of voltage across capacitor C.
$V_{C\rm N}$	Normalized rms voltage across capacitor C.
$V_{\rm d}$	Input dc voltage.
$V_{\rm in,rms}$	RMS value of the fundamental component of input square-wave voltage.
$V_{L,\rm rms}$	RMS value of voltage across inductor L.
$V_{L\rm N}$	Normalized rms voltage across inductor L.
$V_{L_a,\rm rms}$	RMS value of voltage across inductor L_a.
$V_{L_a\rm N}$	Normalized rms voltage across inductor L_a.
$V_{\rm o}$	Output dc voltage.
$Z_{\rm n}$	Characteristic impedance of the resonant circuit.
γ	Ratio of inductors L_a and L.
ϕ	Phase angle between inverter output voltage and current.
ω	$\equiv 2\pi f$, angular switching frequency (in radians per second).
$\omega_{\rm i}$	Normalized switching frequency where H is independent of Q.
$\omega_{\rm n}$	Normalized switching frequency.
$\omega_{\rm o}$	$\equiv 2\pi f_o$, angular resonant frequency (in radians per second).
$\omega_{\rm v}$	Normalized switching frequency where M is independent of Q.

I. INTRODUCTION

RESONANT converters (RCs) feature zero voltage switching (ZVS), zero current switching (ZCS), high-frequency operation, high efficiency, small size, and low electromagnetic interference (EMI). They have been successfully applied to dc power supplies for industrial, commercial, and domestic applications, high-frequency ac power supplies for induction heating, power-factor correction, and discharge lamp ballast. The series [1] and parallel [2] RC (SRC and PRC, respectively) are basic resonant-converter topologies with two reactive elements. The merits of SRC include better part-load efficiency and inherent dc blocking of the isolation transformer due to the series capacitor in the resonant network. However, its part-load regulation is poor and output-voltage regulation at no load is not possible by switching frequency variation. On the other hand, PRC offers no-load regulation but suffers from poor part-load efficiency and lack of inherent dc blocking for the isolation transformer. To remove these limitations, RCs with three and four reactive components were investigated in [3] and [4], respectively.

Manuscript received July 23, 2003; revised March 23, 2005. Abstract published on the Internet September 26, 2005.

The authors are with the Power Supplies Division, Centre for Advanced Technology, Indore 452013, India (e-mail: mbb@cat.ernet.in).

Digital Object Identifier 10.1109/TIE.2005.858729

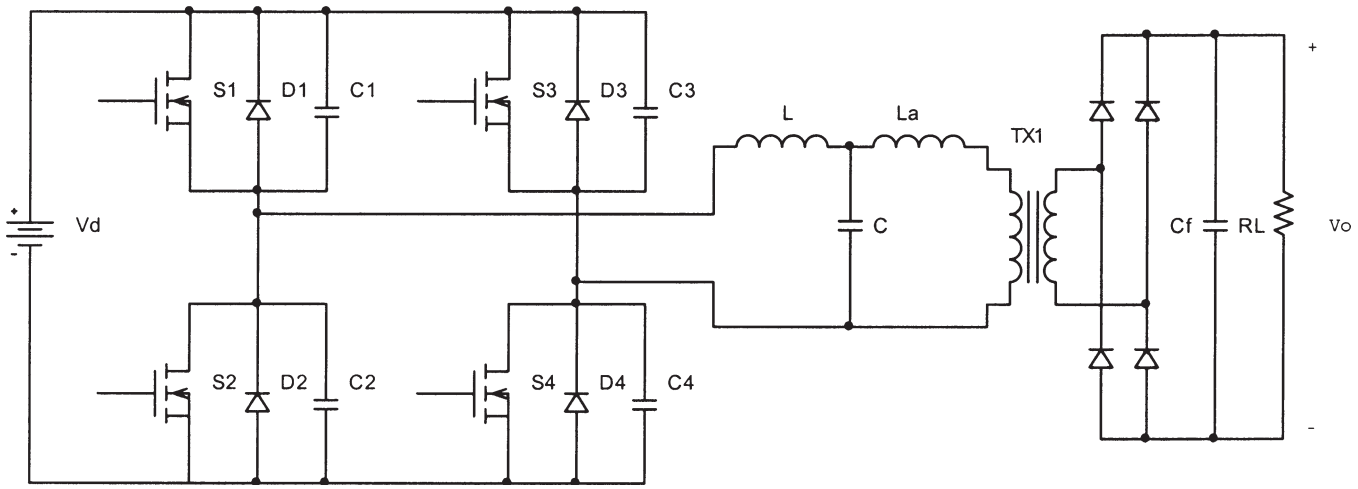

Fig. 1. Circuit diagram of the LCL-T RC.

It has been shown that the addition of an inductor to the SRC significantly improves the no-load-regulation characteristics. The resulting converter, called the LCL RC [5], [6], offers load-independent output voltage when operated at the switching frequency equal to the resonant frequency of the series arm. Therefore, the output voltage can be regulated against wide line and load variations with a moderate sweep of switching frequency. The magnetic components of the RC can also be integrated [7]. Therefore, the LCL RC is deemed as a strong candidate for the output-voltage-regulated power supplies [8].

The addition of an inductor to PRC also changes its characteristics. Because of the T-type resonant network, the resulting topology is referred in this paper as the LCL-T RC. The circuit diagram of this topology is shown in Fig. 1. The LCL-T resonant network composed of inductors L, L_a and capacitor C is driven by a high-frequency full-bridge square-wave inverter. The antiparallel diodes and capacitors shown in Fig. 1 are inherent to each MOSFET switch of the inverter. It has been shown that the LCL-T RC also offers load-independent output voltage and no-load regulation, which is useful for voltage-regulated power supplies [9]. Another interesting property of the LCL-T RC has been pointed out in [10]. When operated at the resonant frequency, the LCL-T RC behaves like a current source. That is, under these conditions, the output current is constant irrespective of load variations. Furthermore, for operation at resonance with $L = L_a$, the inverter output current (that is, current in inductor L) is in phase with the voltage, which further reduces under the part-load condition. This maximizes full-load and part-load converter efficiency due to lower conduction losses. The same property of the LCL-T RC is reported in [11] for realizing a high-power-factor rectifier. The property that the LCL-T RC converts a high-frequency constant-voltage source to a high-frequency constant-current (CC) source using a passive LC element is also signified in [12] and [13].

A CC or an output-current-regulated power supply is required in many commercial, industrial, and research applications such as electromagnets [14], capacitor charging [15], battery charging [16], arc welding [17], semiconductor laser diode drivers [18], etc. The LCL-T RC, by virtue of its current-source property, can become a potential candidate for such application. Although [10]–[13] mention the current-source property of this topology, the detailed analysis, optimization, and design guidelines are not reported in the literature. Therefore, the major objectives of this paper are:

1) to perform a detailed study of the LCL-T RC for its operation as a CC source;
2) to derive and simplify the expressions for voltage and current ratings of different components;
3) present an optimum design of the converter;
4) to validate the analysis with experimental results.

The ac analysis [19] is followed to derive closed-form expressions, discuss the performance characteristics, and derive the condition for optimized design of the converter in Section II. Section III discusses the control-related issues and experimental results on a laboratory prototype are presented in Section IV.

II. Converter Analysis

In the ac analysis, the output rectifier and filter are replaced by the equivalent ac resistance and the square-wave input-voltage source is replaced by its fundamental sinusoidal equivalent. The power transfer from input to output is assumed to be only via the fundamental component and the contribution of all the harmonics is neglected. Without losing generality, the turns ratio (N_1/N_2) of the isolation transformer T_{x1} is assumed to be unity. The equivalent ac resistance for the rectifier with capacitive filter [19] and the rms value of the fundamental component of input square-wave voltage are given by

$$R_{\rm ac} = \frac{8}{\pi^2} R_{\rm L} \quad \text{and} \quad V_{\rm in,rms} = \frac{2\sqrt{2}}{\pi} V_{\rm d}. \tag{1}$$

The resonant frequency and the normalized switching frequency are defined as

$$\omega_{\rm o} = \frac{1}{\sqrt{LC}} \quad \text{and} \quad \omega_{\rm n} = \frac{\omega}{\omega_{\rm o}}. \tag{2}$$

The characteristic impedance and Q of the resonant network are

$$Z_{\rm n} = \sqrt{\frac{L}{C}} \quad \text{and} \quad Q = \frac{\omega_{\rm o} L}{R_{\rm L}} = \frac{Z_{\rm n}}{R_{\rm L}}. \tag{3}$$

The ratio of inductors is defined as

$$\gamma = \frac{L_a}{L}. \tag{4}$$

The voltage and current gain are defined as

$$M = \frac{V_{\rm o}}{V_{\rm d}} \quad \text{and} \quad H = \frac{I_{\rm o}}{\left(\frac{V_{\rm d}}{Z_{\rm n}}\right)}. \tag{5}$$

The voltage gain can be derived as

$$M = \frac{1}{(1-\omega_{\rm n}^2) + j\frac{\pi^2}{8} Q\left[(1+\gamma)\omega_{\rm n} - \gamma\omega_{\rm n}^3\right]}. \tag{6}$$

A close examination of (6) shows that the value of M is independent of load (that is, Q) if

$$\omega_{\rm n} = \omega_{\rm v} = \sqrt{\frac{1+\gamma}{\gamma}} \tag{7}$$

where $\omega_{\rm v}$ is defined as the normalized switching frequency where M is independent of Q. Furthermore, at $\omega_{\rm n} = \omega_{\rm v}$, the converter gain can be expressed as

$$M|_{\omega_{\rm n}=\omega_{\rm v}} = \gamma. \tag{8}$$

Next, the current gain of LCL-T RC can be derived as

$$H = \frac{1}{\frac{1}{Q}\left(1-\omega_{\rm n}^2\right) + j\frac{\pi^2}{8}\left[(1+\gamma)\omega_{\rm n} - \gamma\omega_{\rm n}^3\right]}. \tag{9}$$

We see from (9) that the load current is independent of the load if operated at $\omega_{\rm n} = \omega_{\rm i} = 1$, $\omega_{\rm i}$ being the normalized switching frequency where H is independent of Q. And

$$H|_{\omega_{\rm n}=\omega_{\rm i}} = \frac{8}{\pi^2}. \tag{10}$$

Generalized expressions for normalized voltage and current ratings of different components are derived subsequently. The following base values are defined for the normalization

$$\text{Base voltage} : V_{\rm B} = V_{\rm d} \tag{11}$$

$$\text{Base current} : I_{\rm B} = \frac{V_{\rm d}}{Z_{\rm n}} \tag{12}$$

$$\text{If } A = \left(1-\omega_{\rm n}^2\right) + j\frac{\pi^2}{8} Q\left[(1+\gamma)\omega_{\rm n} - \gamma\omega_{\rm n}^3\right] \tag{13}$$

then

$$I_{LN} = \frac{I_{L,\rm rms}}{I_{\rm B}} = \frac{\pi}{2\sqrt{2}}\left(\frac{Q\left(1-\gamma\omega_{\rm n}^2\right) + j\frac{8}{\pi^2}\omega_{\rm n}}{A}\right) \tag{14}$$

$$I_{CN} = \frac{I_{C,\rm rms}}{I_{\rm B}} = \frac{\pi}{2\sqrt{2}}\left(\frac{-Q\gamma\omega_{\rm n}^2 + j\frac{8}{\pi^2}\omega_{\rm n}}{A}\right) \tag{15}$$

$$I_{L_a\rm N} = \frac{I_{L_a,\rm rms}}{I_{\rm B}} = \frac{\pi}{2\sqrt{2}}\left(\frac{Q}{A}\right) \tag{16}$$

$$V_{LN} = \frac{V_{L,\rm rms}}{V_{\rm B}} = \frac{2\sqrt{2}}{\pi}\left(\frac{-\omega_{\rm n}^2 + j\frac{\pi^2}{8}Q\left(\omega_{\rm n} - \gamma\omega_{\rm n}^3\right)}{A}\right) \tag{17}$$

$$V_{CN} = \frac{V_{C,\rm rms}}{V_{\rm B}} = \frac{2\sqrt{2}}{\pi}\left(\frac{1 + j\frac{\pi^2}{8}Q\gamma\omega_{\rm n}}{A}\right) \tag{18}$$

$$V_{L_a\rm N} = \frac{V_{L_a,\rm rms}}{V_{\rm B}} = \frac{2\sqrt{2}}{\pi}\left(\frac{j\frac{\pi^2}{8}Q\gamma\omega_{\rm n}}{A}\right). \tag{19}$$

For operation at $\omega_{\rm n} = \omega_{\rm i} = 1$, (14) can be simplified as

$$I_{LN}|_{\omega_{\rm n}=\omega_{\rm i}} = \frac{\pi}{2\sqrt{2}}\left(\frac{Q(1-\gamma) + j\frac{8}{\pi^2}}{j\frac{\pi^2}{8}Q}\right). \tag{20}$$

Therefore, the phase angle between the inverter output voltage and current can be derived as

$$\phi|_{\omega_{\rm n}=\omega_{\rm i}} = \tan^{-1}\left(\frac{Q(\gamma-1)}{\frac{8}{\pi^2}}\right) \tag{21}$$

$$\begin{aligned} &\phi|_{\omega_{\rm n}=\omega_{\rm i}} = 0, && \text{if } \gamma = 1 \\ &\phi|_{\omega_{\rm n}=\omega_{\rm i}} < 0, && \text{if } \gamma < 1 \\ &\phi|_{\omega_{\rm n}=\omega_{\rm i}} > 0, && \text{if } \gamma > 1. \end{aligned} \tag{22}$$

Thus, the converter can operate in lagging power-factor mode if $\gamma < 1$. The advantages of an RC operating in lagging power-factor mode are very well known [20]. For the operation in lagging power-factor mode, the antiparallel diode conducts prior to the switch in every cycle to ensure zero voltage turn on. For reliable ZVS of the switch, it is essential that the diode conducts before the switch does. Although $\gamma = 1$ gives a zero phase angle that would result in lowest conduction loss, in practice, the required phase lag can be realized by keeping γ slightly less than unity. Nevertheless, theoretically preferred operating parameters can be decided as $\omega_{\rm n} = 1$ and $\gamma = 1$, and the magnitude of the above-derived expressions can be written in simplified form as below. The resulting error will not be significant as long as γ is close to unity.

$$M|_{\omega_{\rm n}=\gamma=1} = \frac{8}{\pi^2}\left(\frac{1}{Q}\right) \quad \text{and} \quad H|_{\omega_{\rm n}=\gamma=1} = \frac{8}{\pi^2} \tag{23}$$

$$I_{LN}|_{\omega_{\rm n}=\gamma=1} = V_{LN}|_{\omega_{\rm n}=\gamma=1} = \frac{16\sqrt{2}}{\pi^3}\left(\frac{1}{Q}\right) \tag{24}$$

$$I_{L_a\rm N}|_{\omega_{\rm n}=\gamma=1} = V_{L_a\rm N}|_{\omega_{\rm n}=\gamma=1} = \frac{2\sqrt{2}}{\pi} \tag{25}$$

$$I_{CN}|_{\omega_{\rm n}=\gamma=1} = V_{CN}|_{\omega_{\rm n}=\gamma=1} = \frac{2\sqrt{2}}{\pi}\left(\frac{\sqrt{\left(\frac{8}{\pi^2}\right)^2 + Q^2}}{Q}\right). \tag{26}$$

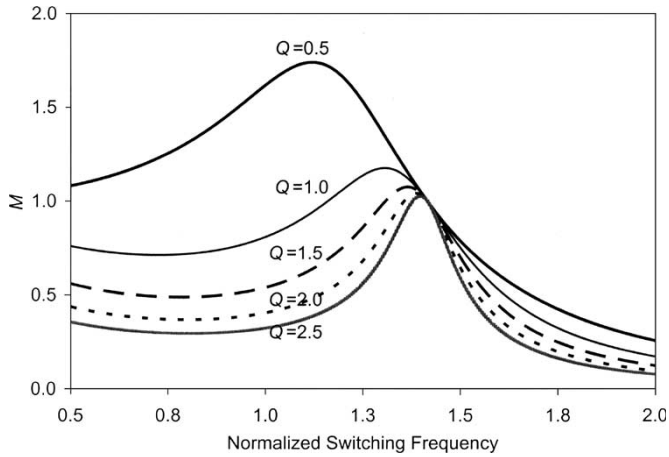

Fig. 2. Converter voltage gain (M) versus normalized switching frequency for $\gamma = 1$.

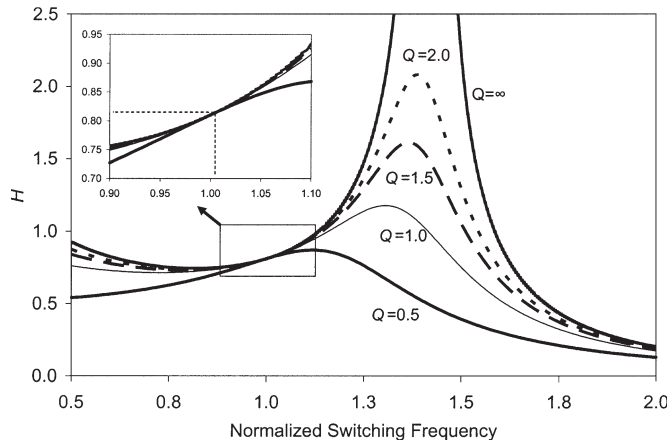

Fig. 3. Converter current gain (H) versus normalized switching frequency for $\gamma = 1$. In the inset: details about the operating point $\omega_{\rm n} = 1$.

Normally, the resonant inductor is a bigger and heavier component than the capacitor. It is known that the physical size of an inductor is indicated by the area product, which is directly proportional to the energy handled by the inductor. The normalized total inductor energy can be derived as

$$E_{\rm n}|_{\omega_{\rm n}=\gamma=1} = \left.\frac{\left(\frac{1}{2}LI^2_{L,\rm rms} + \frac{1}{2}L_aI^2_{L_a,\rm rms}\right)}{\left(\frac{V_{\rm d}^2}{\omega_{\rm o}R_{\rm L}}\right)}\right|_{\omega_{\rm n}=\gamma=1} = \frac{256}{\pi^6}\frac{1}{Q^3} + \frac{4}{\pi^2}\frac{1}{Q}. \quad (27)$$

A. Performance Characteristics

The plots of voltage gain M of LCL-T RC as a function of $\omega_{\rm n}$ are shown in Fig. 2 for $\gamma = 1$. The converter offers load-independent voltage gain at a particular operating frequency; the operating frequency $(\omega_{\rm v})$ and the voltage gain both are functions of γ, as described by (7) and (8). The plots of current gain H are shown in Fig. 3 for different values of Q and $\gamma = 1$. The plot for $Q = \infty$ corresponding to load short circuit is also included to demonstrate current-source behavior. H is seen to be load independent at $\omega_{\rm n} = \omega_i = 1$ under all conditions. The region around $\omega_{\rm n} = 1$ in Fig. 3 is magnified and shown as inset. It can be noticed that the load current is nearly independent of load even for operation in the vicinity of $\omega_{\rm n} = 1$. This can be achieved by keeping full-load $Q \geq 1$. At no load, the load resistance is 0 for a current-source power supply or, in other words, at no load, $Q = \infty$. Note from (24) that under the no-load condition, the inverter output current is 0. This shows that the input current reduces proportionately from full load to no load and thus, the converter maintains excellent efficiency.

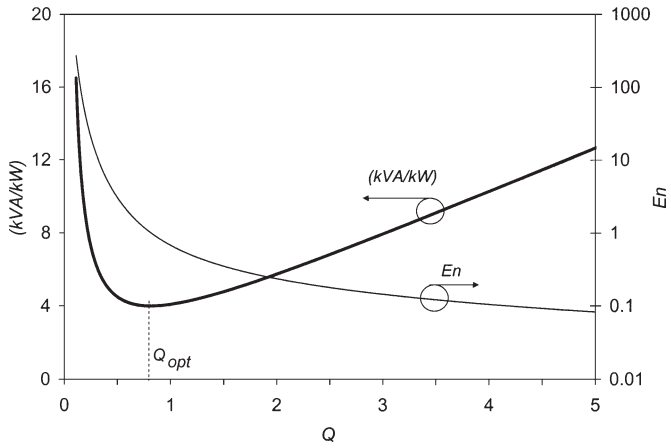

Fig. 4. (kVA/kW) and $E_{\rm n}$ rating of the LCL-T RC as a function of Q for $\gamma = 1$ and $\omega_{\rm n} = 1$.

B. Optimization

The reactive components in a RC increase its size. Therefore, the RCs are optimized for minimum size of resonant network. The (kVA/kW) rating of resonant network is considered as an index for the physical size of the resonant network. Using expressions (23)–(26), the (kVA/kW) rating of LCL-T RC can be derived from

$$\left.\frac{\rm kVA}{\rm kW}\right|_{\omega_{\rm n}=\gamma=1} = \left.\frac{V_{CN}\cdot I_{CN} + V_{LN}\cdot I_{LN} + V_{L_a\rm N}\cdot I_{L_a\rm N}}{M\cdot H}\right|_{\omega_{\rm n}=\gamma=1}. \quad (28)$$

The plot of (28) is shown in Fig. 4 as a function of Q for $\gamma = 1$ and $\omega_{\rm n} = 1$. The plot shows the existence of a particular value of Q where (kVA/kW) is minimum. This is termed as the optimum value of Q $(Q_{\rm opt})$. It can be shown that $Q_{\rm opt} = (8/\pi^2)$. For the design of the converter, full-load Q should be taken equal to $Q_{\rm opt}$. Also shown in Fig. 4 is the normalized total inductor energy $E_{\rm n}$, which decreases with increase in Q.

III. Converter Control

Although the output current of LCL-T RC is seen to be constant irrespective of changes in the load, for practical application as a current-source power supply, it should be possible to regulate the output current against input-voltage variations. In some applications, wide conversion range is desired. Since the LCL-T RC behaves as a current source only when operated

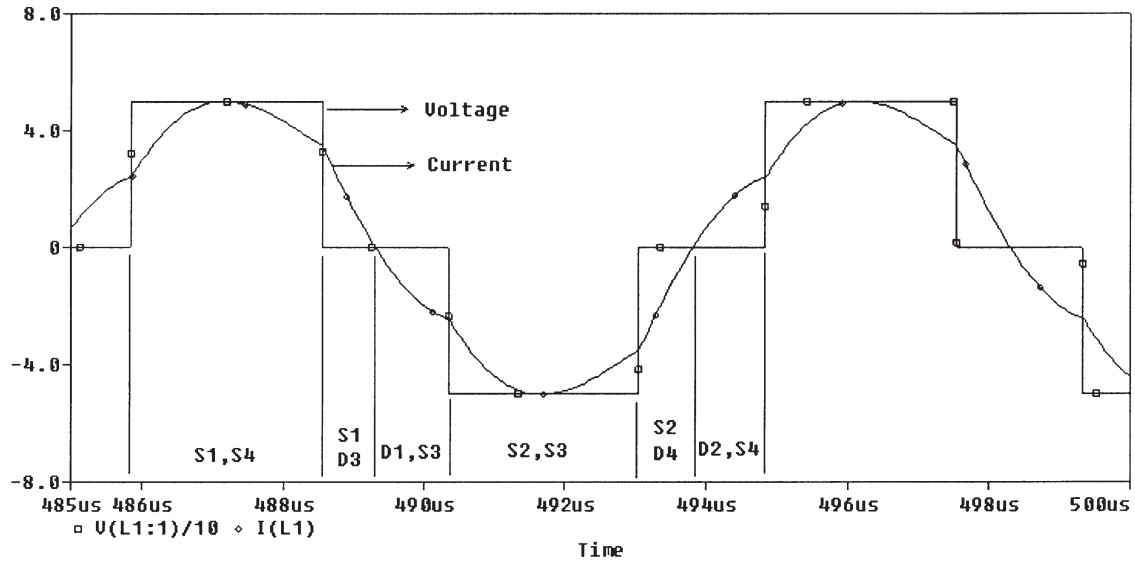

Fig. 5. Simulated waveforms of inverter output voltage and current with clamped-mode control. Also shown are the devices conducting in various subintervals.

at $\omega_{\rm n} = 1$, the method using variation of switching frequency to control the output cannot be applied—or else current-source behavior will be lost. Besides, Fig. 3 shows that the current gain characteristics is relatively flat in the vicinity of $\omega_{\rm n} = 1$. Thus, variation of switching frequency will not provide wide conversion range and output-current regulation against large input-voltage variations. Constant frequency control must therefore be applied. Various fixed-frequency control strategies for SRC have been reported in the literature [21], [22], namely, clamped-mode (CM) control, asymmetrical duty-cycle (ADC) control, and asymmetrical voltage cancellation (AVC) control. They can be applied to the LCL-T RC. Loss of ZVS of the switches under certain operating conditions may be a limitation of these methods. Illustratively, Fig. 5 shows simulated waveforms of inverter output voltage and current with CM control for operation with $\omega_{\rm n} = 1$, $\gamma = 1$, and $Q = Q_{\rm opt}$. Since the LCL-T RC is designed to operate in unity or slightly lagging power-factor mode of operation, the ZVS of switches in the bridge inverter is seen to be lost with CM control. The ZVS of switches is expected to be maintained over a wider range of operation with ADC and AVC control than with the CM control. However, ADC and AVC control methods necessitate a capacitor in series with L to block the dc component of high-frequency excitation voltage resulting from the asymmetrical operation.

Alternatively, the output current of the LCL-T RC can be varied over a wide range by controlling its input dc voltage by a front-end converter, which can be a soft switching PWM topology—with or without isolation. The second stage is the LCL-T RC free running at $\omega_{\rm n} = 1$. This method allows flexibility in the design. The resonant network can be designed with optimum parameters for maximum efficiency. However, two cascaded converters reduce the overall conversion efficiency and increase complexity, component count, and cost.

Since LCL-T RC is a current source, it lends itself for easy paralleling without any additional care for equal current sharing. A parallel connection of low-power modules instead of a single high-power converter is known to provide modularity, standardization, redundancy, and high reliability. With transformer-isolated LCL-T RC, two or more modules can be connected in parallel. Furthermore, if the operation of two modules is phase shifted, the average total output current is doubled and the peak–peak ripple is reduced. It can be shown that for two paralleled modules, the ripple will be minimum, equal to 32.53% of average total current, when the phase shift between two modules is 90°. Similarly, for three modules, the ripple will be minimum, equal to 14.03%, when the phase shift is 60° or 120°. The peak–peak ripple will be 7.81% and 4.97% for four and five parallel-connected phase-shifted modules, respectively. In general, the optimum phase shift among the modules is given by $(180/p)$ degrees, where p is the number of paralleled connected modules. The per-unit peak–peak ripple as a function of phase shift is shown in Fig. 6 for different values of p. The graph assumes sinusoidal current waveshape. For p modules in parallel, the ripple frequency of output as well as input current will be $2p$ times the switching frequency. The filtering requirement is thus significantly reduced, and in some applications, filter can be eliminated.

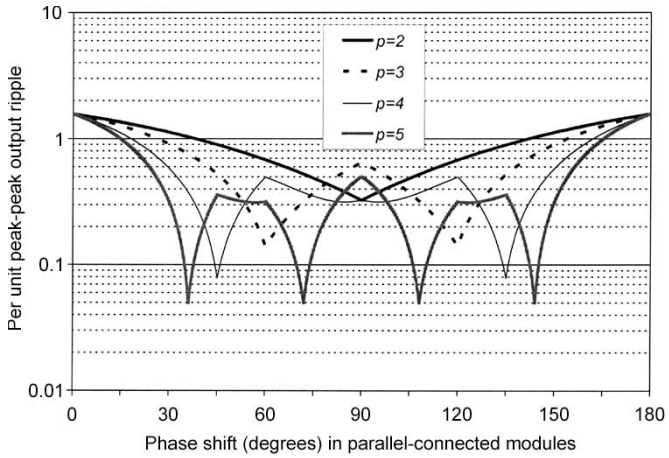

Fig. 6. Parallel operation of LCL-T RC modules: The per-unit peak–peak ripple as a function of phase shift. p is the number of paralleled modules.

TABLE I
DESIGN PARAMETERS FOR THE EXPERIMENTAL CONVERTER

Parameter	Value
L (μH)	14.47
L_a (μH)	14.47
C (μF)	0.141
N_1/N_2	5
$I_{L,rms}$ (A)	4.45
$I_{La,rms}$ (A)	4.45
$I_{C,rms}$ (A)	6.28
$V_{L,rms}$ (V)	45
$V_{La,rms}$ (V)	45
$V_{C,rms}$ (V)	63

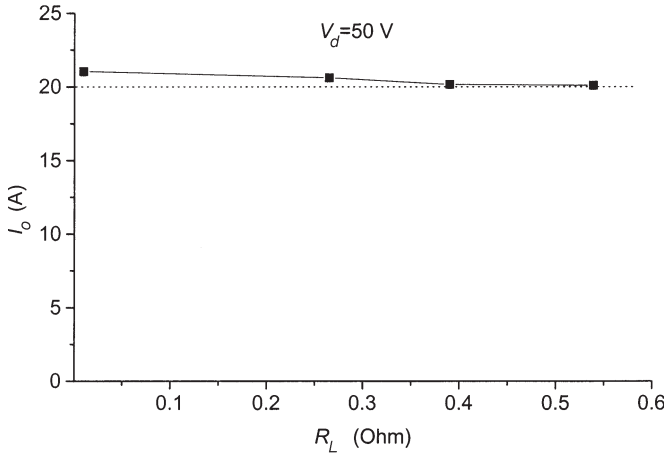

Fig. 7. Open-loop output characteristics of the prototype experimental converter.

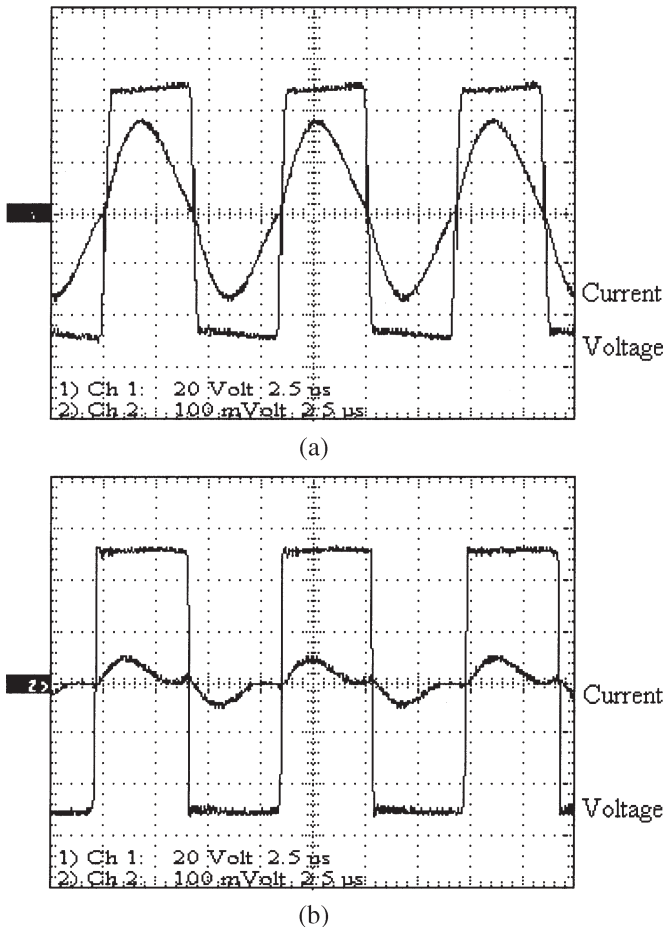

Fig. 8. Voltage and current waveforms at the output of the inverter bridge. (a) $R_{\rm L} = 0.53\ \Omega$, and, (b) $R_{\rm L} = 0.1\ \Omega$. Scale: 20 V/div (voltage), 5 A/div (current), and 2.5 μs/div.

IV. EXPERIMENTAL RESULTS

A laboratory prototype of the LCL-T RC dc current-source power supply is designed, built, and tested to validate the current-source property of the LCL-T RC. The converter has the following specifications: input dc supply voltage = 50 V, maximum output current = 20 A, maximum load resistance (full load) = 0.5 Ω, and switching frequency = 100 kHz. In the analysis of previous sections, the transformer turns ratio (N_1/N_2) was assumed to be unity. In the design procedure to follow, the transformer is included. The previous results still apply; however, they are scaled suitably by transformer turns ratio. The optimum value of Q is derived as

$$Q_{\rm opt} = \frac{8}{\pi^2} = \frac{\omega_{\rm o} L}{R_{\rm L}\left(\frac{N_1}{N_2}\right)^2} = \frac{Z_{\rm n}}{R_{\rm L}\left(\frac{N_1}{N_2}\right)^2}. \tag{29}$$

Rewriting (10)

$$I_{\rm o} = \frac{8}{\pi^2}\left(\frac{V_{\rm d}}{Z_{\rm n}}\right)\left(\frac{N_1}{N_2}\right). \tag{30}$$

From (29) and (30)

$$\frac{N_1}{N_2} = \frac{V_{\rm d}}{I_{\rm o} R_{\rm L}}. \tag{31}$$

In the present design example, $N_1/N_2 = 5$. Then, the values of L and C can be calculated as 16.11 μH and 0.157 μF, respectively, for the design with $Q = Q_{opt}$ at full load and resonant frequency of 100 kHz. However, 0.157 μF is an odd value and could not be realized with available capacitors. Connecting three 0.047-μF capacitors in parallel, the closest realizable value is 0.141 μF. Accordingly, the value of L is scaled to 14.47 μH to retain equal $Z_{\rm n}$. The resonant and switching frequency is consequently changed to 111.43 kHz. The component values and their computed ratings at full load are summarized in Table I. The input bridge inverter is realized with 200-V MOSFET switches. A secondary center-tap transformer is used to reduce losses in the output rectifier stage. A common-cathode Schottky module rated for 45 V and 40 A is used for output rectification. A 20-μF capacitor forms the output filter in the prototype. The measured transformer leakage inductance reflected on the primary side was 2.5 μH. Hence, an additional 11.5-μH inductance is added to make $L_a = 14$ μH. $L = 14.5$ μH, resulting in γ slightly less than unity. In fact, to reduce the circuit components, the leakage inductance of the transformer can be beneficially used as the resonant inductor L_a. Various techniques allow predictable and controlled leakage inductance in a transformer [23]–[25].

Fig. 7 shows the open-loop output characteristics of the prototype converter. The converter operates at a 50-V dc input. The load was varied from short-circuit condition to full load. The output current is seen to be approximately constant

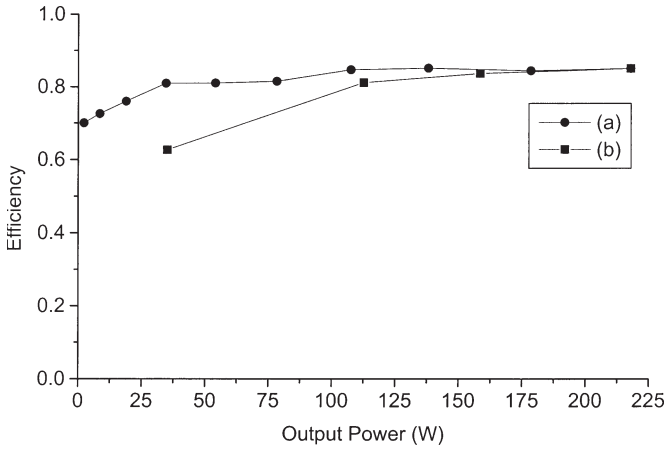

Fig. 9. Efficiency of the experimental converter as a function of output power. Plot (a): $R_{\rm L} = 0.53\ \Omega$ and $V_{\rm d}$ is varied from 5 to 50 V. Plot (b): $V_{\rm d} = 50$ V and load resistance is varied.

at 20 A. The slight droop in the characteristics is due to the increase in conduction losses in the bridge inverter and resonant network. The voltage and current waveforms at the output of the inverter bridge are shown in Fig. 8(a) and (b) for $R_{\rm L} = 0.53$ and $0.1\ \Omega$, respectively. Besides being in phase with the voltage, the inverter output current is seen to reduce with load, as predicted in the analysis, resulting in high part-load efficiency. Fig. 9 shows the experimental converter efficiency as a function of output power. In plot (a), $R_{\rm L} = 0.53\ \Omega$ and input dc voltage is varied from 5 V to 50 V. This plot indicates high efficiency over the entire conversion range. The maximum efficiency is 0.85 at 217-W output power, which drops to 0.7 when the output power is reduced to 2.25 W. The highest efficiency is limited to 0.85 because drops in the circuit (output rectifier and MOSFETs) become comparable with the low output voltage (10 V) of the experimental prototype. Plot (b) shows the efficiency of the experimental converter when operated at 50-V input and load resistance is varied to change the output power.

V. Conclusion

A detailed analysis of the LCL-T RC is presented in this paper for its application as a CC power supply. Closed-form expressions for converter gain and component stresses are derived. It is seen that the converter exhibits load-independent voltage and current gain at certain operating frequencies, the latter being useful for a CC power supply. The condition for converter design optimized for minimum size of resonant network is derived. Various methods for the control of output current over a wide conversion range and against variation in input dc voltage are discussed. Being an inherent current source, the converter lends itself for easy paralleling without any complex control for equal current sharing. If the paralleled modules are phase shifted, the peak–peak ripple in output and input currents is reduced and the ripple frequency is increased. This reduces the filtering requirement. If sufficient number of modules are connected in parallel, the additional filter can be eliminated. The leakage inductance of the transformer can be advantageously integrated into the LCL-T resonant network. Part-load efficiency is better due to lower circulating currents. Experimental results on the prototype converter validates the merits of the converter topology. These merits make the topology applicable as a CC power supply in various applications.

References

[1] V. Vorperian and S. Cuk, "A complete dc analysis of series resonant converter," in *Proc. IEEE Power Electronics Specialists Conf. (PESC)*, Cambridge, MA, 1982, pp. 85–100.

[2] A. K. S. Bhat and M. M. Swamy, "Analysis and design of high frequency parallel resonant converter operating above resonance," in *Proc. IEEE Applied Power Electronics Conf. and Expo. (APEC)*, New Orleans, LA, 1988, pp. 182–189.

[3] R. P. Severns, "Topologies for three-element resonant converters," *IEEE Trans. Power Electron.*, vol. 7, no. 1, pp. 89–98, Jan. 1992.

[4] I. Bataresh, "Resonant converter topologies with three and four energy storage elements," *IEEE Trans. Power Electron.*, vol. 9, no. 1, pp. 64–73, Jan. 1994.

[5] A. Bhat, "Analysis and design of LCL-type series resonant converter," *IEEE Trans. Ind. Electron.*, vol. 41, no. 1, pp. 118–124, Feb. 1994.

[6] M. Borage, S. Tiwari, and S. Kotaiah. (2001, Mar. 5). Design optimization of LCL-type series resonant converter. *PowerPulse*, Corona, CA: Darnell.Com Inc. [Online]. Available: http://www.powerpulse.net/features/techpaper.php?paperID=76

[7] B. Yang, R. Chen, and F. Lee, "Integrated magnetics for LLC resonant converter," in *Proc. IEEE Applied Power Electronics Conf. and Expo. (APEC)*, Dallas, TX, 2002, pp. 346–351.

[8] M. Borage, S. Tiwari, and S. Kotaiah, "Comparison of three element VNV resonant converters," in *Proc. India Int. Conf. Power Electronics (IICPE)*, Mumbai, India, 2002.

[9] C. Chakraborty, M. Ishida, and Y. Hori, "Performance and design of an L-C-L converter for voltage regulator type applications," *Trans. IEE Jpn.*, vol. 119-D, no. 6, pp. 848–856, Jun. 1999.

[10] H. Pollock, "Simple constant frequency constant current load-resonant power supply under variable load conditions," *IEE Electron. Lett.*, vol. 33, no. 18, pp. 1505–1506, Aug. 1997.

[11] H. Seidel, "A high power factor tuned class D converter," in *Proc. IEEE Power Electronics Specialists Conf. (PESC)*, Kyoto, Japan, 1988, pp. 1038–1042.

[12] H. Irie and H. Yamana, "Immittance converter suitable for power electronics," *Trans. IEE Jpn.*, vol. 117D, no. 8, pp. 962–969, 1997.

[13] ——, "Immittance converter suitable for power electronics," *Electr. Eng. Jpn. (Scripta Technica, Inc. and s/p scripta publishing company)*, vol. 124, no. 2, pp. 53–62, 1998.

[14] F. Bonaudi, "Magnets in particle physics," in *Proc. CERN Accelerator School Magnetic Measurement and Alignment*, Montreux, Switzerland, 1992, pp. 1–14.

[15] A. C. Lippincott and R. M. Nelms, "A capacitor charging power supply using a series resonant topology, constant on-time/variable frequency control and zero-current switching," *IEEE Trans. Ind. Electron.*, vol. 38, no. 6, pp. 438–447, Dec. 1991.

[16] C. Simpson. (1995). *Battery charging*, Santa Clara CA: National Semiconductors. [Online]. Available: http://www.national.com/appinfo/power/files/f7.pdf

[17] *Welding Handbook Vol. 2—Welding Processes*, 3rd ed. R. O'Brien, Ed. Miami, FL: American Welding Society, Feb. 1992.

[18] M. K. Koli, S. R. Tiwari, and M. B. Borage, "QCW laser diode driver—pulsed current sources," in *Proc. DAE-BRNS National Laser Symp. (NLS)*, Indore, India, 2002, pp. 175–176.

[19] R. Steigerwald, "Comparison of half-bridge resonant converter topologies," *IEEE Trans. Power Electron.*, vol. PEL-3, no. 2, pp. 174–182, Apr. 1988.

[20] ——, "High frequency resonant transistor dc–dc converters," *IEEE Trans. Ind. Electron.*, vol. IE-31, no. 2, pp. 181–191, May 1984.

[21] F. Monterde, J. Burlo, P. Hernandez, and J. Garcia, "Unipolar voltage cancellation control of resonant inverters for induction cooking appliances," in *Proc. IEEE Industrial Electronics, Control, and Instrumentation (IECON)*, Aachen, Germany, 1998, pp. 820–824.

[22] J. Burdio, F. Canales, P. Barbosa, and F. Lee, "Comparison of fixed-frequency control strategies for ZVS dc/dc series resonant converter," in *Proc. Center Power Electronics Systems (CPES) Seminar*, Blacksburg, VA, 2002, pp. 182–186.

[23] A. Kats, G. Ivensky, and S. Ben-Yaakov, "Application of integrated magnetics in resonant converters," in *Proc. IEEE Applied Power Electronics Conf. and Expo. (APEC)*, Atlanta, GA, 1987, pp. 925–931.
[24] M. Meinhardt, M. Duffy, T. O'Donell, S. Reilly, J. Flannery, and C. O'Mathuna, "New method of integration of resonant inductor and transformer: Design, realization and measurements," in *Proc. IEEE Applied Power Electronics Conf. and Expo. (APEC)*, Dallas, TX, 1999, pp. 1168–1174.
[25] C. Chakraberty, M. Ishida, and T. Hori, "Novel half-bridge resonant converter topology realized by adjusting transformer parameters," *IEEE Trans. Ind. Electron.*, vol. 49, no. 1, pp. 197–205, Jan. 2002.

Mangesh Borage received the B.E. degree in electrical engineering from Shivaji University, Kolhapur, India, in 1993, and the M.Tech. degree in electrical engineering with specialization in power electronics from Banaras Hindu University, Varanasi, India, in 1996.

He joined the 38th batch of the training school at Bhabha Atomic Research Centre (BARC), Mumbai, India, in 1994. Since 1995, he has been with the Centre for Advanced Technology (CAT), Indore, India, as a Scientific Officer, where he is primarily responsible for the development of high-stability current-regulated power supplies for electromagnets used in research and medical particle accelerators. His research interests include soft switching and resonant converters, power-factor correction, high-frequency magnetic components, and high-frequency power converters, in general.

Mr. Borage is recipient of University Merit Certificate from Shivaji University, Kolhapur, India, for First Rank in Electrical Engineering in 1993. He was also the recipient of the Dr. Homi Bhabha Award at BARC, Mumbai, India, in 1995. He is an Associate Member of Institution of Engineers, India, and a Life Member of the Society of EMC Engineers, India (SEMCEI), the Indian Society for Particle Accelerators (ISPA), and the Society of Indian Power Electronics Professionals.

Sunil Tiwari received the B.E. degree in electronics engineering from Maharaja Sayajirao University, Vadodra, India, in 1984.

He was with Bharat Heavy Electricals Limited (BHEL), Bangalore, India, from 1984 to 1987 and with the Ministry of Defense, Agra, India from 1987 to 1989. Since 1989, he has been with the Centre for Advanced Technology (CAT) Indore, India, as a Scientific Officer. His research interests include soft switching and resonant techniques for high-power application and development of high-stability power supplies for particle accelerators.

Mr. Tiwari is a Member of the Institution of Engineers, India, and a Life Member of the Society of EMC Engineers, India (SEMCEI), the Indian Society for Particle Accelerators (ISPA), and the Indian Nuclear Society (INS).

Swarna Kotaiah received the B.E. degree in electronics and communication engineering from Andhra University, Waltair, India, in 1973.

He joined 17th batch of the Training School at Bhabha Atomic Research Centre (BARC), Mumbai, India, in 1973. From 1974 to 1986, he was with Variable Energy Cyclotron Centre (VECC), Kolkata, India, and worked in the fields of power supplies, radio-frequency amplifiers, and instrumentation. Since 1986, he bas been with the Centre for Advanced Technology (CAT), Indore, India, where he is the Head of the Power Supplies Division and the Project Manager for Indus-2 Synchrotron Radiation Source. His research areas include power electronics, instrumentation, and high-power high-stability precision power supplies.

Mr. Kotaiah is a Life Member of the Indian Vacuum Society (IVS) and the Indian Society for Particle Accelerators (ISPA).

射 频 和 天 线 设 计 培 训 课 程 推 荐

易迪拓培训(www.edatop.com)由数名来自于研发第一线的资深工程师发起成立，致力并专注于微波、射频、天线设计研发人才的培养；我们于 2006 年整合合并微波 EDA 网(www.mweda.com)，现已发展成为国内最大的微波射频和天线设计人才培养基地，成功推出多套微波射频以及天线设计经典培训课程和 ADS、HFSS 等专业软件使用培训课程，广受客户好评；并先后与人民邮电出版社、电子工业出版社合作出版了多本专业图书，帮助数万名工程师提升了专业技术能力。客户遍布中兴通讯、研通高频、埃威航电、国人通信等多家国内知名公司，以及台湾工业技术研究院、永业科技、全一电子等多家台湾地区企业。

易迪拓培训课程列表：http://www.edatop.com/peixun/rfe/129.html

射频工程师养成培训课程套装

该套装精选了射频专业基础培训课程、射频仿真设计培训课程和射频电路测量培训课程三个类别共 30 门视频培训课程和 3 本图书教材；旨在引领学员全面学习一个射频工程师需要熟悉、理解和掌握的专业知识和研发设计能力。通过套装的学习，能够让学员完全达到和胜任一个合格的射频工程师的要求…

课程网址：http://www.edatop.com/peixun/rfe/110.html

ADS 学习培训课程套装

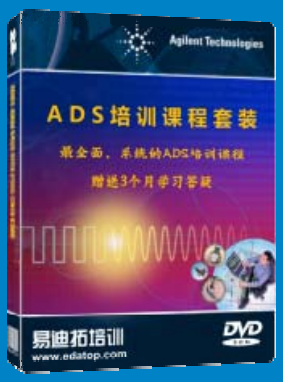

该套装是迄今国内最全面、最权威的 ADS 培训教程，共包含 10 门 ADS 学习培训课程。课程是由具有多年 ADS 使用经验的微波射频与通信系统设计领域资深专家讲解，并多结合设计实例，由浅入深、详细而又全面地讲解了 ADS 在微波射频电路设计、通信系统设计和电磁仿真设计方面的内容。能让您在最短的时间内学会使用 ADS，迅速提升个人技术能力，把 ADS 真正应用到实际研发工作中去，成为 ADS 设计专家...

课程网址： http://www.edatop.com/peixun/ads/13.html

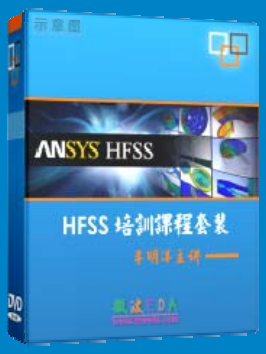

HFSS 学习培训课程套装

该套课程套装包含了本站全部 HFSS 培训课程，是迄今国内最全面、最专业的 HFSS 培训教程套装，可以帮助您从零开始，全面深入学习 HFSS 的各项功能和在多个方面的工程应用。购买套装，更可超值赠送 3 个月免费学习答疑，随时解答您学习过程中遇到的棘手问题，让您的 HFSS 学习更加轻松顺畅…

课程网址：http://www.edatop.com/peixun/hfss/11.html

CST 学习培训课程套装

该培训套装由易迪拓培训联合微波 EDA 网共同推出，是最全面、系统、专业的 CST 微波工作室培训课程套装，所有课程都由经验丰富的专家授课，视频教学，可以帮助您从零开始，全面系统地学习 CST 微波工作的各项功能及其在微波射频、天线设计等领域的设计应用。且购买该套装，还可超值赠送 3 个月免费学习答疑…

课程网址：http://www.edatop.com/peixun/cst/24.html

HFSS 天线设计培训课程套装

套装包含 6 门视频课程和 1 本图书，课程从基础讲起，内容由浅入深，理论介绍和实际操作讲解相结合，全面系统的讲解了 HFSS 天线设计的全过程。是国内最全面、最专业的 HFSS 天线设计课程，可以帮助您快速学习掌握如何使用 HFSS 设计天线，让天线设计不再难…

课程网址：http://www.edatop.com/peixun/hfss/122.html

13.56MHz NFC/RFID 线圈天线设计培训课程套装

套装包含 4 门视频培训课程，培训将 13.56MHz 线圈天线设计原理和仿真设计实践相结合，全面系统地讲解了 13.56MHz 线圈天线的工作原理、设计方法、设计考量以及使用 HFSS 和 CST 仿真分析线圈天线的具体操作，同时还介绍了 13.56MHz 线圈天线匹配电路的设计和调试。通过该套课程的学习，可以帮助您快速学习掌握 13.56MHz 线圈天线及其匹配电路的原理、设计和调试…

详情浏览：http://www.edatop.com/peixun/antenna/116.html

我们的课程优势：

※ 成立于 2004 年，10 多年丰富的行业经验，

※ 一直致力并专注于微波射频和天线设计工程师的培养，更了解该行业对人才的要求

※ 经验丰富的一线资深工程师讲授，结合实际工程案例，直观、实用、易学

联系我们：

※ 易迪拓培训官网：http://www.edatop.com

※ 微波 EDA 网：http://www.mweda.com

※ 官方淘宝店：http://shop36920890.taobao.com